

## DYNAMICAL FRICTION IN A GASEOUS MEDIUM

EVE C. OSTRIKER

Department of Astronomy, University of Maryland, College Park, MD 20742-2421

Received 1998 August 3; accepted 1998 October 6

### ABSTRACT

Using time-dependent linear perturbation theory, we evaluate the dynamical friction force on a massive perturber  $M_p$  traveling at velocity  $V$  through a uniform gaseous medium of density  $\rho_0$  and sound speed  $c_s$ . This drag force acts in the direction  $-\hat{V}$  and arises from the gravitational attraction between the perturber and its wake in the ambient medium. For supersonic motion ( $\mathcal{M} \equiv V/c_s > 1$ ), the enhanced-density wake is confined to the Mach cone trailing the perturber; for subsonic motion ( $\mathcal{M} < 1$ ), the wake is confined to a sphere of radius  $c_s t$  centered a distance  $Vt$  behind the perturber. Inside the wake, surfaces of constant density are hyperboloids or oblate spheroids for supersonic or subsonic perturbers, respectively, with the density maximal nearest the perturber. The dynamical drag force has the form  $F_{\text{DF}} = -I \times 4\pi(GM_p)^2 \rho_0 / V^2$ . We evaluate  $I$  analytically; its limits are  $I \rightarrow \mathcal{M}^3/3$  for  $\mathcal{M} \ll 1$ , and  $I \rightarrow \ln(Vt/r_{\text{min}})$  for  $\mathcal{M} \gg 1$ . We compare our results to the Chandrasekhar formula for dynamical friction in a collisionless medium, noting that the gaseous drag is generally more efficient when  $\mathcal{M} > 1$ , but is less efficient when  $\mathcal{M} < 1$ . To allow simple estimates of orbit evolution in a gaseous protogalaxy or proto-star cluster, we use our formulae to evaluate the decay times of a (supersonic) perturber on a near-circular orbit in an isothermal  $\rho \propto r^{-2}$  halo, and of a (subsonic) perturber on a near-circular orbit in a constant-density core. We also mention the relevance of our calculations to protoplanet migration in a circumstellar nebula.

*Subject headings:* hydrodynamics — ISM: general — shock waves

### 1. INTRODUCTION

The process of dynamical friction (DF), defined as momentum loss by a massive moving object due to its gravitational interaction with its own gravitationally induced wake, arises in many astronomical systems. Examples of systems in which such effects are known to be important include stars in clusters or galaxies, galaxies in galaxy clusters, and binary star cores in the common envelope phase of evolution. In the first two examples, the surrounding background medium in general consists of a combination of collisionless matter (stars, galaxies, dark matter) and gas, while in the third example the surrounding medium is entirely gaseous. In all these cases, as a corollary to the DF process, the background medium is heated at an equal and opposite rate to the energy lost by the perturber.

The analytic theory for the gravitational drag in collisionless systems was developed by Chandrasekhar (1943), and over the decades since, it has enjoyed widespread theoretical application, extensive verification by numerical experiments, and well-documented embodiment in observed astronomical systems. The variety of important consequences of gravitational drag in collisionless astronomical systems includes mass segregation in star clusters, sinking satellites in dark matter galaxy halos, orbital decay of binary supermassive black holes after galaxy mergers, etc.; see, e.g., Binney & Tremaine (1987).

Less well developed is the corresponding theory of DF in a gaseous (i.e., collisional) medium.<sup>1</sup> For supersonic motion, analytic linear theory estimates of the gravitational drag

under assumption of a steady state were obtained by Dokuchaev (1964), Ruderman & Spiegel (1971), and Rephaeli & Salpeter (1980). The resulting estimates for the drag force in the steady supersonic case take the form

$$F_{\text{ss}} = \frac{4\pi(GM_p)^2 \rho_0}{V^2} \ln\left(\frac{r_{\text{max}}}{r_{\text{min}}}\right), \quad (1)$$

where  $r_{\text{max}}$  and  $r_{\text{min}}$  correspond, respectively, to the effective linear sizes of the surrounding medium and the perturbing object, similar to the drag formula obtained for a collisionless medium. Although there is some ambiguity in the definition of  $r_{\text{max}}$  and  $r_{\text{min}}$ , the estimate (eq. [1]) appears consistent with calculations of the gravitational drag that are obtained as a by-product of numerical hydrodynamic investigations focused on the Bondi-Hoyle-Lyttleton accretion problem; see, e.g., Shima et al. (1985), Shankar, Kley, & Burkert (1993), and Ruffert and collaborators (see Ruffert 1996, and references therein).

For steady state, subsonic motion of the perturber, the front-back symmetry of the perturbed density distribution about the perturber led Rephaeli & Salpeter (1980) to argue that gravitational drag is absent in the subsonic, inviscid case. Considering that the drag force for the supersonic case increases proportionally to  $V^{-2}$  with decreasing perturber speed  $V$ , it seems counterintuitive for the dynamical drag to become exactly zero when  $V$  becomes infinitesimally smaller than the sound speed. In this paper, we reconsider the linear-theory drag as a time-dependent rather than a steady state problem, and we arrive instead at a nonzero value for the DF for the subsonic case while still verifying that the drag force is maximized for perturbers with  $V \approx c_s$ . In § 2 we derive results for the perturbed density distributions created by, and dynamical drag on, a massive perturber on a constant-velocity trajectory through a uniform, infinite medium. In § 3 we relate our results to the classical

<sup>1</sup> Instead, most studies of the gravitational interaction between a moving massive body and the surrounding gaseous medium have focused on the problem of accretion, following on the analysis of Hoyle & Lyttleton (1939), Bondi & Hoyle (1944), and the early numerical work of Hunt (1971).

(collisionless) DF formula, and we briefly consider applications to a few astronomical systems.

## 2. ANALYSIS

### 2.1. Wave Equation and Formal Solution using Green's Functions

We begin with the linearized equations for the perturbed density  $\rho \equiv \rho_0[1 + \alpha(x, t)]$  and velocity  $\mathbf{v} \equiv c_s \beta(x, t)$  of an adiabatic gaseous medium that is subject to an external gravitational potential  $\Phi_{\text{ext}}(x, t)$ :

$$\frac{1}{c_s} \frac{\partial \alpha}{\partial t} + \nabla \cdot \beta = 0, \quad (2)$$

and

$$\frac{1}{c_s} \frac{\partial \beta}{\partial t} + \nabla \alpha = -\frac{1}{c_s^2} \nabla \Phi_{\text{ext}}, \quad (3)$$

where  $\rho_0$  is the unperturbed density,  $c_s \equiv (\partial P_0 / \partial \rho_0)^{1/2}$  is the sound speed, and the perturbation amplitudes  $\alpha, |\beta| \ll 1$ . By substituting equation (2) in the divergence of equation (3), we have

$$\nabla^2 \alpha - \frac{1}{c_s^2} \frac{\partial^2 \alpha}{\partial t^2} = -\frac{1}{c_s^2} \nabla^2 \Phi_{\text{ext}} \equiv -4\pi f(x, t), \quad (4)$$

where  $\rho_{\text{ext}}(x, t) \equiv [c_s^2 f(x, t)]/G$  is the mass density of the perturber.

In the absence of any disturbance prior to the action of  $\Phi_{\text{ext}}$ , the solution to equation (4) is found using the retarded Green's function  $G^+$  for the three-dimensional wave equation (§ 6.6 of Jackson 1975) as

$$\alpha(x, t) = \iint d^3x' dt' \frac{\delta[t' - (t - |\mathbf{x} - \mathbf{x}'|/c_s)] f(\mathbf{v}', t')}{|\mathbf{x} - \mathbf{x}'|}. \quad (5)$$

### 2.2. Perturbed Density Distributions for Constant-Velocity Perturbers

We now specialize to the case of a point mass  $M_p$  on a straight-line trajectory with velocity  $V\hat{z}$ , passing at time  $t = 0$  through  $\mathbf{x} = 0$ . If  $\mathcal{H}(t)$  describes the time over which the perturber is active, then  $f(x, t) = (GM_p/c_s^2)\delta(z - Vt)\delta(x)\delta(y)\mathcal{H}(t)$ . We define  $s \equiv z - Vt$  as the distance along the line of motion relative to the perturber,  $w \equiv z' - z$ , and  $\mathcal{M} \equiv V/c_s$  as the Mach number;  $w > 0$  ( $< 0$ ) corresponds to the perturbation from a backward (forward) propagating wave. Then,

$$\alpha(x, t) = \frac{GM_p}{c_s^2} \int_{-\infty}^{\infty} dw \times \frac{\delta[w + s + \mathcal{M}(R^2 + w^2)^{1/2}]\mathcal{H}((w + z)/V)}{(R^2 + w^2)^{1/2}}. \quad (6)$$

Here  $R = (x^2 + y^2)^{1/2}$  is the cylindrical radius.

To evaluate the integral (eq. [6]), one expands the argument of the  $\delta$ -function about its possible roots:

$$w_{\pm} = \frac{s \pm \mathcal{M}[s^2 + R^2(1 - \mathcal{M}^2)]^{1/2}}{\mathcal{M}^2 - 1}; \quad (7)$$

for  $\mathcal{M} < 1$ , only  $w_+$  is a valid root, whereas for  $\mathcal{M} > 1$  both roots are valid as long as  $s < 0$  and  $|s|/R > (\mathcal{M}^2 - 1)^{1/2}$ ,

and neither otherwise. Using  $\delta((w - w_{\pm})A) = \delta(w - w_{\pm})/|A|$  for  $A = 1 + \mathcal{M}w_{\pm}/(R^2 + w_{\pm}^2)^{1/2}$  and substituting the solution given by equation (7), the result is

$$\alpha = \frac{GM_p/c_s^2}{[s^2 + R^2(1 - \mathcal{M}^2)]^{1/2}} \sum_{\text{roots } w_0} \mathcal{H}\left(\frac{z + w_0}{V}\right). \quad (8)$$

For a purely steady solution over all time,  $\mathcal{H}$  is unity for all arguments, with the result that

$$\alpha_s = \frac{GM_p/c_s^2}{[s^2 + R^2(1 - \mathcal{M}^2)]^{1/2}}$$

$$\times \begin{cases} 1 & \text{if } \mathcal{M} < 1, \\ 2 & \text{if } \mathcal{M} > 1 \text{ and } s/R < -(\mathcal{M}^2 - 1)^{1/2}, \\ 0 & \text{otherwise.} \end{cases} \quad (9)$$

This confirms the analytic linear theory results of previous authors for completely steady flow created by a point mass on a straight-line, constant-speed trajectory:

1. A subsonic perturber generates a density distribution centered on the perturber at  $s = 0$ , with contours of constant density corresponding to similar ellipses in the  $s$ - $R$  plane with eccentricity  $e = \mathcal{M}$ , and the short axis along the line of motion of the perturber (i.e., the three-dimensional density distribution consists of concentric similar oblate spheroids). The density contrast  $\rho_1/\rho_0 \equiv \alpha$  is unity for an elliptical section with semiminor axis  $GM_p/c_s^2$ ; the linearization is sensible only outside of this elliptical section. This density distribution is a generalization of the far-field limit of the hydrostatic envelope  $\rho/\rho_0 = \exp[GM_p/(c_s^2 r)]$  that surrounds a stationary perturber.<sup>2</sup>

2. A supersonic perturber generates a density wake only within the rear Mach cone of half-opening angle  $\sin \theta = 1/\mathcal{M}$  defined by  $s/R < -(\mathcal{M}^2 - 1)^{1/2}$ ; the surfaces of constant density within the wake correspond to hyperbolae in the  $s$ - $R$  plane, with eccentricity  $e = \mathcal{M}$ .

Now consider the case where the perturber is “turned on” at  $t = 0$ , so that  $\mathcal{H}$  is a Heaviside function. For a subsonic perturber  $\mathcal{M} < 1$ , the only root is  $w_+$  (eq. [7]). Algebraic calculation shows that for  $\mathcal{M} < 1$ ,  $z + w_+ > 0$  when  $R^2 + z^2 < (c_s t)^2$ . Thus the region of perturbation is the sphere centered on the original position of the perturber, within which a sound wave has traveled in time  $t$ . Within this region of perturbation, the density distribution has reached the value given by the steady solution (eq. [9]); outside the causal region for sound waves, the density remains unperturbed.

For a supersonic perturber, any density disturbance must be confined within the rear Mach cone  $s/R < -(\mathcal{M}^2 - 1)^{1/2}$ . Algebraic calculation shows that within the sphere  $R^2 + z^2 < (c_s t)^2$ ,  $z + w_+ > 0$  and  $z + w_- < 0$ ; hence only  $w_+$  contributes in equation (8). Within the Mach cone and to the right [ $R < |z - \mathcal{M}c_s t|/(\mathcal{M}^2 - 1)^{1/2}$ ,  $z > c_s t/\mathcal{M}$ ] of this sphere [ $R^2 + z^2 > (c_s t)^2$ ], both  $z + w_+$  and

<sup>2</sup> We note that for subsonic flow, the far-field density enhancement from eq. (9) is within 10% of Hunt's (1971)  $\mathcal{M} = 0.6$  numerical solution outside of  $r = GM_p/c_s^2$ . Also, the rms anisotropy of 7% from the far-field steady solution (eq. [9]) with  $\mathcal{M} = 0.6$  is comparable to the 5% mean anisotropy cited for Hunt's (1971) near-field numerical solution.

$z + w_-$  are real and positive, and hence contribute in equation (8).

The results for the perturbed density for this finite-time perturbation are summarized as follows:<sup>3</sup>

$$\alpha(t) = \frac{GM_p/c_s^2}{[s^2 + R^2(1 - \mathcal{M}^2)]^{1/2}}$$

$$\times \begin{cases} 1 & \text{if } R^2 + z^2 < (c_s t)^2, \\ 2 & \text{if } \mathcal{M} > 1, R^2 + z^2 > (c_s t)^2, \\ & s/R < -(\mathcal{M}^2 - 1)^{1/2}, \text{ and } z > c_s t/\mathcal{M}, \\ 0 & \text{otherwise.} \end{cases} \quad (10)$$

The region of perturbed density has the shape of a loaded ice cream cone dragged by its point by the perturber  $M_p$ ;

<sup>3</sup> These results appear to have been obtained previously by Just & Kegel (1990) via an alternative mathematical formalism; the two calculations serve as independent checks of the formulae.

only  $w_+$  contributes in the ice cream region (region 1), while both  $w_{\pm}$  contribute in the cone region (region 2). The cone shrinks in size as  $\mathcal{M}$  decreases for  $\mathcal{M} > 1$ , and is nonexistent for  $\mathcal{M} < 1$ . Figures 1 and 2 show examples of the perturbed density distributions for subsonic and supersonic perturbers, respectively. Because of the linear-theory assumptions made at the outset, we note that equation (10) is properly valid only for  $\alpha \ll 1$ ; i.e.,  $s^2 + R^2(1 - \mathcal{M}^2) \gg (GM_p/c_s^2)^2$ .

### 2.3. Gravitational Drag Formulae

To compute the gravitational drag on the perturber, we need to evaluate the gravitational force between the perturber and its wake,

$$F_{\text{DF}} = 2\pi GM_p \rho_0 \iint ds dR R \frac{\alpha(t)s}{(s^2 + R^2)^{3/2}}. \quad (11)$$

To perform the volume integral, it is convenient to transform to a spherical polar coordinate system  $(r, \theta)$  centered on the massive perturber, with  $R \equiv r \sin \theta$  and  $s \equiv r \cos \theta$ .

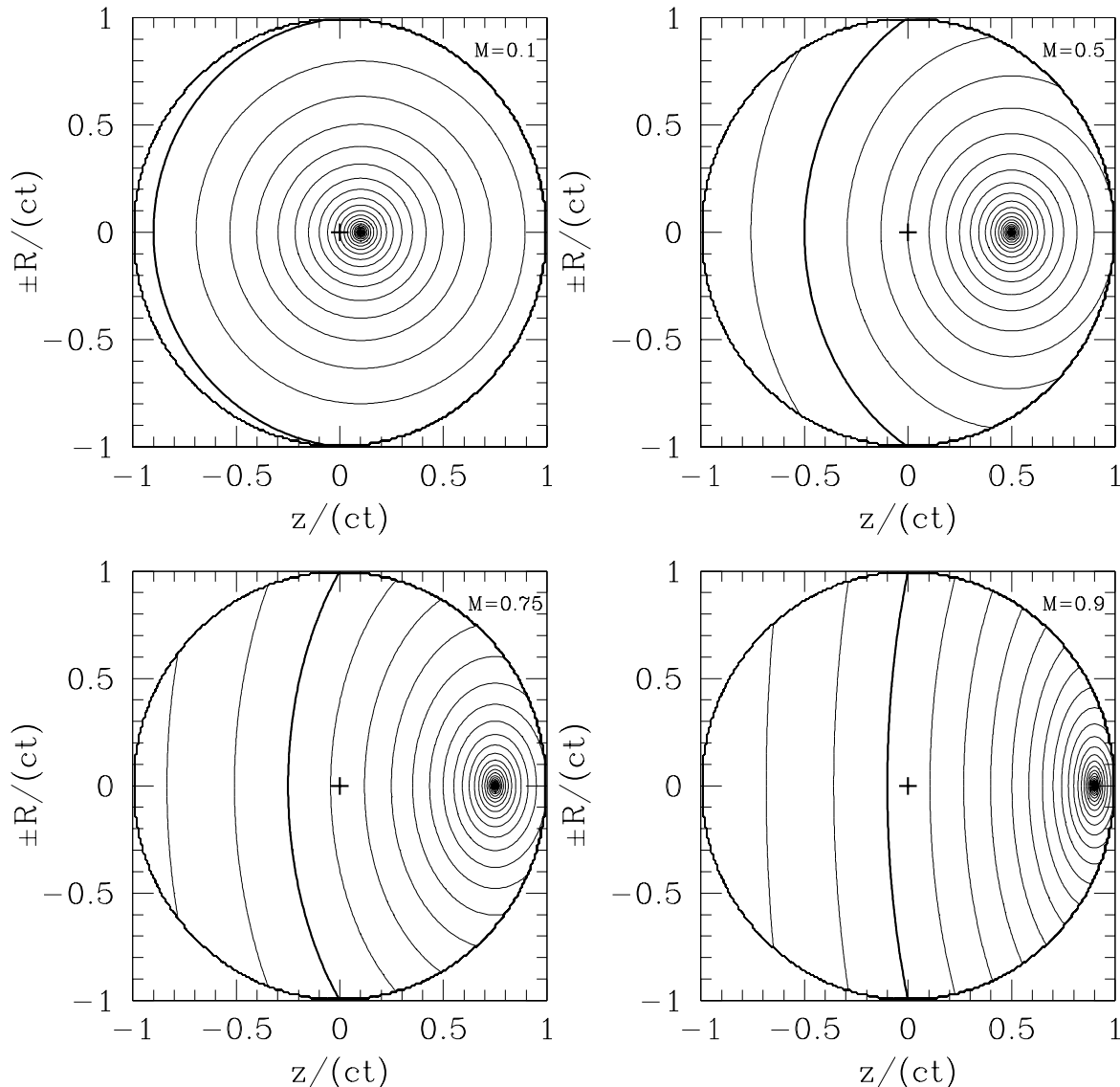


FIG. 1.—Density perturbation profiles for subsonic perturbers with  $\mathcal{M} = 0.1, 0.5, 0.75$ , and  $0.9$  (as indicated at upper right). Contours show isosurfaces of  $\log(\tilde{\alpha}) = \log(\alpha) - \log[GM_p/(tc_s^2)]$  in intervals of  $0.1$ . Density increases toward the perturber; the heavy contour indicates the surface with  $\tilde{\alpha} = 1$ . The plus symbol indicates the initial position of the perturber.

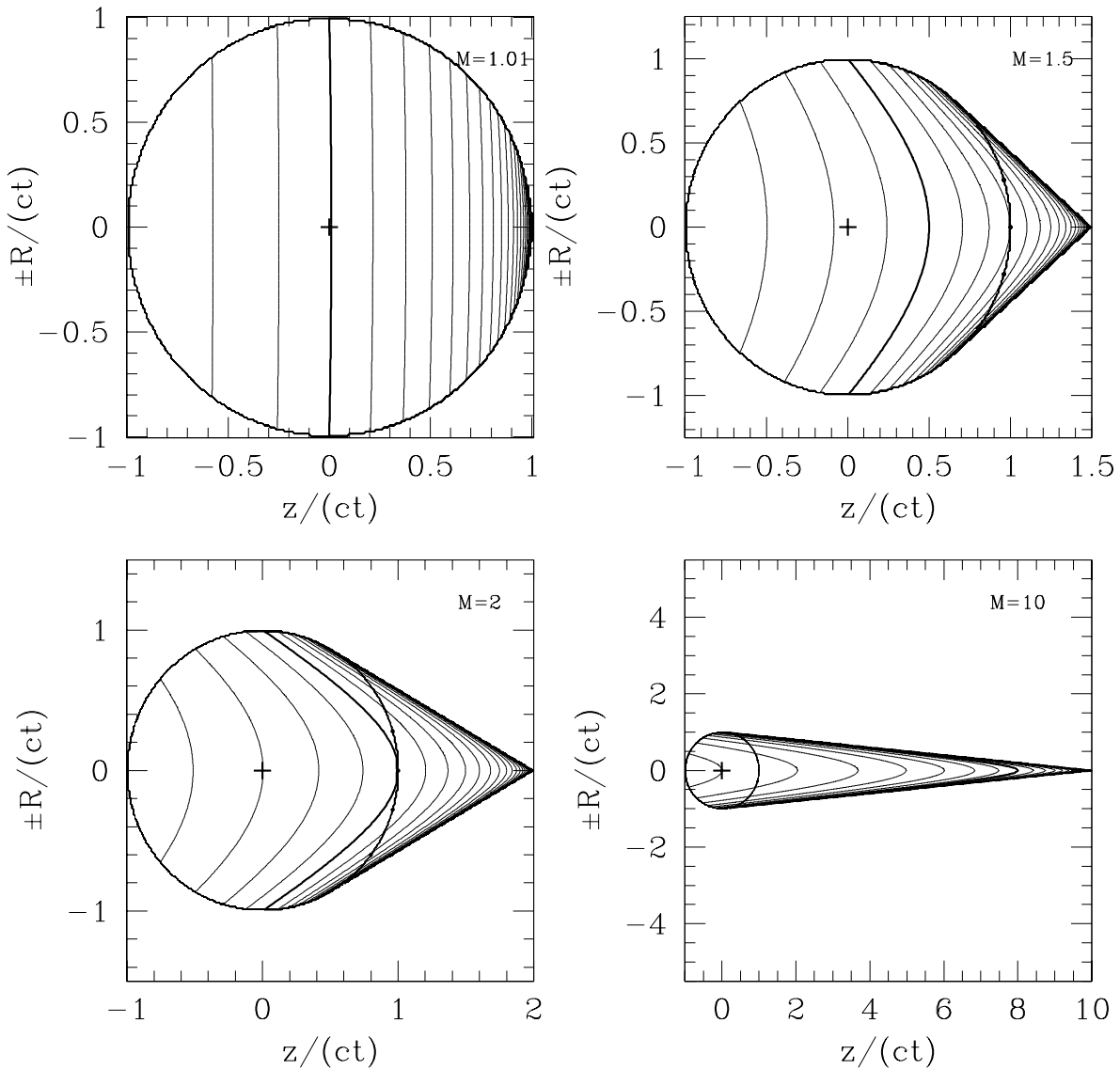


FIG. 2.—Density perturbation profiles for supersonic perturbors with  $\mathcal{M} = 1.01, 1.5, 2,$  and  $10$  (as indicated at upper right). Contours show isosurfaces of  $\log(\tilde{\alpha}) = \log(\alpha) - \log[GM_p/(tc^3)]$  in intervals of  $0.1$ . Density increases toward the perturber at the apex of the Mach cone. The heavy contour indicates the surface with  $\tilde{\alpha} = 1$ . There is a density jump with  $\Delta \log \alpha = \log 2 = 0.301$  at the surface  $R^2 + z^2 = (c_s t)^2$ . The plus symbol indicates the initial position of the perturber.

Defining  $\mu = \cos \theta, x \equiv r/c_s t$ , we have

$$F_{\text{DF}} = -\mathcal{F}I, \quad \mathcal{F} \equiv \frac{4\pi(GM_p)^2 \rho_0}{V^2}, \quad (12)$$

where

$$I = -\frac{1}{2} \int \frac{dx}{x} \int d\mu \frac{\mu \mathcal{M}^2 \mathcal{S}_{\mathcal{M}}}{(1 - \mathcal{M}^2 + \mu^2 \mathcal{M}^2)^{1/2}}. \quad (13)$$

Here  $\mathcal{S}_{\mathcal{M}}$  represents the sum in equation (8).

For the purely steady state density perturbation given in equation (9), in the subsonic case  $\mathcal{S}_{\mathcal{M}} = 1$  everywhere in space, and front-back antisymmetry in the angle integral (due to the symmetric spheroidal density distribution) argues that there is zero net force on the perturber. For the steady state, supersonic case,  $\mathcal{S}_{\mathcal{M}} = 2$  for all  $\mu$  between  $-1$  and  $\mu_{\mathcal{M}} \equiv -(\mathcal{M}^2 - 1)^{1/2}/\mathcal{M}$  (the boundary of the Mach cone), so that  $I = \int dx/x \equiv \ln(r_{\text{max}}/r_{\text{min}})$ . This is consistent

with previous results and yields an identical formula to that representing the DF force in a collisionless medium when  $V$  is much larger than the background particle velocity dispersion (see, e.g., eq. [7-18] of Binney & Tremaine 1987).

For the finite-time case based on the perturbed density distribution in equation (10), there is nonzero contribution to the integral  $I$  only from a finite region in space: region 1, in which  $\mathcal{S}_{\mathcal{M}} = 1$ , and region 2, in which  $\mathcal{S}_{\mathcal{M}} = 2$ . Region 2 is nonexistent for subsonic perturbors. For the subsonic case, the perturber is surrounded by a concentric distribution of similar ellipsoids and is displaced by  $Vt$  forward from the center of the sonic sphere (radius  $c_s t$ ) surrounding its initial position. The nearby, complete ellipsoids exert no net force on the perturber, but the larger, cut-off ones with semiminor axes between  $(c_s - V)t$  and  $(c_s + V)t$  lag behind the perturber (see Fig. 1) and exert a gravitational drag. Thus the radial integral in equation (13) has upper/lower limits  $x = 1 \pm \mathcal{M}$ , and the angular integral has limits  $\mu = -1, \mu_{\mathcal{C}}$ ,

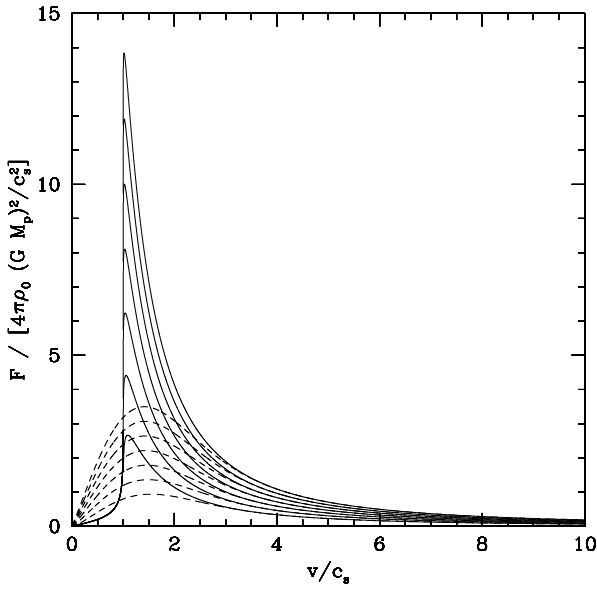


FIG. 3.—*Solid lines*: DF force in a gaseous medium as a function of Mach number  $\mathcal{M} = V/c_s$ . Curves correspond to  $\ln(c_s t/r_{\min}) = 4, 6, 8, \dots, 16$ . *Dashed lines*: Corresponding DF force in a collisionless medium with particle velocity dispersion  $\sigma = c_s$  and  $r_{\max} \equiv Vt = \mathcal{M}c_s t$ .

with  $\mu_C \equiv (1 - \mathcal{M}^2 - x^2)/(2x\mathcal{M})$ . The integrals are straightforward; the result is

$$I_{\text{subsonic}} = \frac{1}{2} \ln\left(\frac{1 + \mathcal{M}}{1 - \mathcal{M}}\right) - \mathcal{M}. \quad (14)$$

The implicit assumptions in deriving this equation are that  $(c_s - V)t$  exceeds the effective size of the perturber ( $r_{\min}$ ), and that  $(c_s + V)t$  is smaller than the effective size of the surrounding gaseous medium ( $r_{\max}$ ). Under these conditions, the dynamical drag is time independent and nonzero. The steady state result that zero net force results from the front-back symmetry of the density distribution is misleading; because of the long-range nature of the Coulomb potential, the total drag force at any time depends on the unchanging ratio  $(c_s t + vt)/(c_s t - vt) = (1 + \mathcal{M})/(1 - \mathcal{M})$  between the semiminor axes of the furthest and closest perturbing *partial* spheroids. The gravitational drag is always dominated by the far field, and at any time the perturber is located ahead of center of the sonic sphere. Physically, we can associate the energy loss arising from the drag force with the rate at which the expanding sound wave does work on the background medium. In the limit of a very slow perturber  $\mathcal{M} \ll 1$ ,  $I_{\text{subsonic}} \rightarrow \mathcal{M}^3/3$ , so that the drag force is proportional to the perturber's speed  $V$ .

For the supersonic case, the whole of the perturbed density distribution lags the perturber. The angular integration limits are  $\mu = -1, \mu_{\mathcal{M}}$  for  $x = r_{\min}/(c_s t)$  to  $(\mathcal{M}^2 - 1)^{1/2}$ , and  $\mu = -1, \mu_C$  for  $x = (\mathcal{M}^2 - 1)^{1/2}$  to  $\mathcal{M} + 1$ ;  $\mathcal{L}_{\mathcal{M}}$  takes on values 2 and 1 in regions 2 and 1. The result of the integration is

$$\begin{aligned} I_{\text{supersonic}} &= \frac{1}{2} \ln\left(\frac{\mathcal{M} + 1}{\mathcal{M} - 1}\right) + \ln\left(\frac{\mathcal{M} - 1}{r_{\min}/c_s t}\right) \\ &= \frac{1}{2} \ln\left(1 - \frac{1}{\mathcal{M}^2}\right) + \ln\left(\frac{Vt}{r_{\min}}\right). \end{aligned} \quad (15)$$

We have assumed that  $Vt - c_s t > r_{\min}$ , and that the effective size of the background medium exceeds  $Vt + c_s t$ . In

the limit  $\mathcal{M} \gg 1$ , we have  $I_{\text{supersonic}} \rightarrow \ln(Vt/r_{\min})$ ; with  $Vt \rightarrow r_{\max}$ , this recovers the steady state result.<sup>4</sup>

In Figure 3, we plot the DF force as a function of the Mach number for several values of  $c_s t/r_{\min}$ .

### 3. DISCUSSION

The main formal result of this paper is the evaluation, in linear perturbation theory, of the gravitational drag force  $F_{\text{DF}}$  on a massive perturber  $M_p$  moving on a straight-line trajectory through an infinite, homogeneous, gaseous medium of density  $\rho_0$  and sound speed  $c_s$ . Together with the definition in equation (12), equations (14) and (15) give the DF drag forces on subsonic and supersonic perturbers, respectively. Figure 3 presents the same results graphically, showing how the drag force varies with the Mach number  $\mathcal{M}$  of the perturber, and the time over which the perturber has been moving with fixed speed  $V = c_s \mathcal{M}$ .

For comparison, we have also included in Figure 3 the result for the gravitational drag on a particle of mass  $M_p$  moving through a collisionless medium with the same density  $\rho_0$  as the gaseous medium we have considered, and with a Maxwellian distribution of particle velocities with  $\sigma = c_s$ . From equation (7-18) of Binney & Tremaine (1987), the collisionless DF drag force is given by equation (12) with

$$I_{\text{collisionless}} = \ln\left(\frac{r_{\max}}{r_{\min}}\right) \left[ \text{erf}(X) - \frac{2X}{\sqrt{\pi}} e^{-X^2} \right], \quad (16)$$

where  $X \equiv V/(\sigma\sqrt{2})$ . From Figure 3, it is clear that (1) for  $\mathcal{M} \gg 1$ , the collisionless and gaseous DF forces are identical (as has been previously noted); (2) for  $\mathcal{M} < 1$ , the drag force is generally larger in a collisionless medium than in a gaseous medium, because in the latter case pressure forces create a symmetric distribution in the background medium in the vicinity of the perturber; (3) the functional form of the gaseous DF drag is much more sharply peaked near  $\mathcal{M} = 1$  than it is for the collisionless DF drag—perturbers moving at speeds near Mach 1 resonantly interact with the pressure waves that they launch in the background medium; and (4) for a given value of  $\ln(\Lambda) \equiv \ln(r_{\max}/r_{\min})$ , the peak value of the gaseous DF force is much larger than the corresponding peak value of the collisionless DF force; at  $\mathcal{M} \approx 1$ , there is a factor of 4 difference in the force between the two cases. We explore some potential consequences of these results in a variety of astronomical systems below.

As a consequence of the stronger gaseous DF force than collisionless DF drag force for supersonic motion, massive objects may make their way more rapidly to the center of a star cluster or galaxy if they arrive at the outer edge before, rather than after, the gas is turned into stars. For a particular example, we consider the decay of a massive perturber's near-circular orbit in a spherical density distribution with a singular isothermal sphere profile  $\rho(r) = c_s^2/(2\pi Gr^2)$ , so  $M(r) = 2c_s^2 r/G$  (here  $c_s$  denotes the sound speed or the velocity dispersion for a gaseous or stellar distribution, respectively). For this density profile, the circular speed is constant,  $V = c_s\sqrt{2}$ . By equating the rate of decrease of angular momentum  $d(M_p Vr)/dt$  to the torque  $\tau_{\text{DF}} = rF_{\text{DF}}$ ,

<sup>4</sup> As pointed out by the referee S. Tremaine, the notion that the maximum impact parameter increases as  $Vt$  was earlier introduced by Ostriker & Davidsen (1968) in a time-dependent analysis of stellar relaxation.

one finds that the time for the perturber's orbit to decay from  $r_{\text{init}}$  to  $r \ll r_{\text{init}}$  is given approximately by

$$\frac{t_{\text{DF}}(r_{\text{init}})}{t_{\text{orb}}(r_{\text{init}})} \approx \frac{M(r_{\text{init}})}{4\pi M_p \ln(r/r_{\text{min}})} \quad (17)$$

for gaseous DF. This time is a factor of 0.428 shorter than the corresponding decay time under stellar DF (see, e.g., eq. [7–25] of Binney & Tremaine 1987). For galactic applications, the implication is that condensed objects that form early (e.g., globular clusters) could spiral into the galactic center from a factor of 1.5 farther in a galaxy than would be predicted by stellar DF theory (Tremaine, Ostriker, & Spitzer 1975), within the epoch over which the baryonic distribution remains gaseous. For star cluster applications, the shorter DF time for gaseous distributions may help explain why young, embedded stellar clusters like the Orion nebular cluster (Hillenbrand 1997; Hillenbrand & Hartmann 1998) appear significantly more relaxed than expected from stellar DF alone; e.g., for the Orion nebular cluster,  $n$ -body simulations show that stellar DF would require a time a factor of 3–4 longer than the best estimate of the cluster age to establish the observed mass segregation (Marshall, Ostriker, & Teuben 1999).

As mentioned above (see Fig. 3), the gaseous DF force is strongly depressed for subsonic perturbers. For modeling the *global* evolution of combined star-gas systems in which the particle velocity dispersion and gas sound speed are comparable, the strong cutoff of  $F_{\text{DF}}$  for subsonic perturbers implies that setting  $F_{\text{DF}} = 0$  for  $V < c_s$  (see, e.g., Saiyadpour, Deiss, & Kegel 1997) should yield realistic results. However, in other circumstances it is interesting to inquire how the small, but nonzero, DF drag on subsonic perturbers (computed in this paper) can affect their orbit evolution.

As a model problem, we consider the decay of a subsonically moving mass  $M_p$  on a near-circular orbit embedded within a constant-density gaseous sphere of radius  $r_0$ . For constant background density, the angular orbit frequency  $\Omega = (4\pi G\rho_0/3)^{1/2}$  and orbital period  $t_{\text{orb}} = 2\pi/\Omega$  are independent of the distance  $r$  from the center. If this constant-density region represents the core of a nonsingular isothermal sphere with core radius  $r_0$  and sound speed  $c_s$ , then  $r_0\Omega/c_s = 3^{1/2}$ ; thus the Mach number for a circular orbit at  $r$  is  $\mathcal{M} = 3^{1/2}r/r_0$ . Just as above for decay in a power-law density profile, we can compute the time for the perturber's orbit to decay from  $r_{\text{init}} = r_0/3^{1/2}$  to  $r_f$  as

$$\frac{t(r_f)}{t_{\text{orb}}} = \frac{M_{\text{core}}}{\pi 3^{5/2} M_p} \int_{\mathcal{M}_f = \sqrt{3}r_f/r_0}^1 \frac{\mathcal{M} d\mathcal{M}}{I_{\text{subsonic}}(\mathcal{M})}; \quad (18)$$

the numerical coefficient equals 0.0204.

Figure 4a shows how the decay of the orbital radius depends on time and on the mass of the perturber relative to the whole core. In Figure 4b, we verify that the assumption of a near-circular orbit is valid provided  $M_p/M_{\text{core}} \ll 1$ , since

$$\frac{v_r}{v_\phi} = \frac{3^{5/2} M_p I_{\text{subsonic}}(\mathcal{M})}{2M_{\text{core}} \mathcal{M}^3}, \quad (19)$$

which has the limit  $2.598M_p/M_{\text{core}}$  for  $\mathcal{M} \ll 1$ . In arriving at the results shown in Figure 4, we have used equation (14). Its validity depends, however, on the size of the uniform-density core exceeding that of the perturbed-density region.

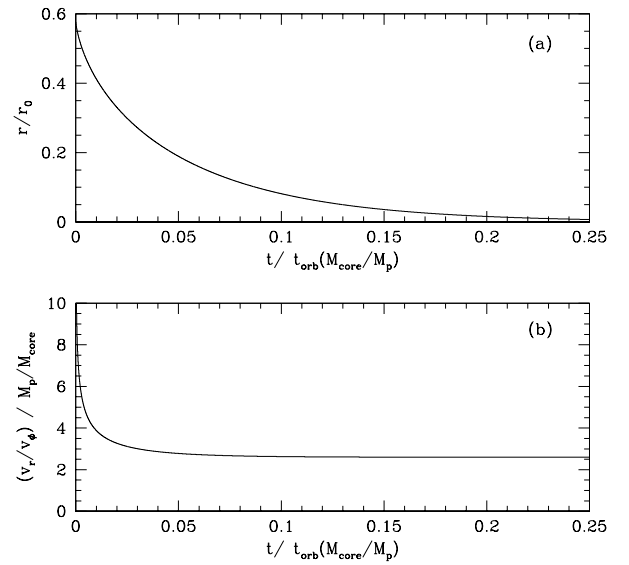


FIG. 4.—(a) Decay in time of radial distance  $r$  of massive perturber  $M_p$  on near-circular orbit about the center of uniform-density core of mass  $M_{\text{core}}$ , radius  $r_0$ , and sound speed  $c_s = [GM_{\text{core}}/(3r_0)]^{1/2}$ . (b) Radial-to-azimuthal velocity ratio for the same situation, as in (a).

This assumption must fail, and the DF drag force consequently decrease, when the forward wave defining the disturbed-density region (e.g., Fig. 1) reaches a distance  $\sim r_0$  ahead of the perturber.<sup>5</sup> The position  $r(t_{\text{fw}})$  of the perturber at this time is plotted as a function of  $M_p/M_{\text{core}}$  in Figure 5. Based on this figure, only perturbers of mass  $M_p > 0.2M_{\text{core}}$  are predicted to reach within 1/10 of a core radius before the DF drag decreases. For lower mass perturbers, this implies that the decay of orbits to very small radii may stall if the DF drag is sharply reduced after the time  $t_{\text{fw}}$ . This result may have relevance for models of QSO evolution (Silk & Rees 1998) in which primordial black holes are formed away from the centers of galaxies to later be driven there by DF during mergers. If, as assumed in this scenario, these events occur before the advent of star formation, then the relevant DF drag is the gaseous DF examined in this paper.

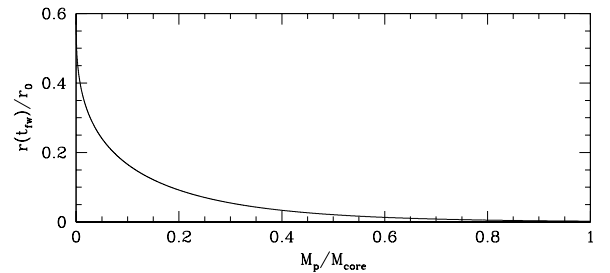


FIG. 5.—For the same situation as in Fig. 4, perturber's radial distance from the center at time when the forward wave disturbance has propagated ahead of the perturber by  $r_0$  (see text).

<sup>5</sup> Because the perturber follows a circular rather than straight-line orbit, the DF drag at late times should still be nonzero: since the direction of  $\vec{V}$  changes by  $\pi/2$  four times per orbit, the forward-wave propagation effectively “restarts” as well. When  $r \ll r_0$ , over each quarter-orbit each new expansion wave propagates to just  $\sim r_0$ ; over much of the quarter-orbit an unbalanced trailing density enhancement will remain within the core. Thus we expect that the DF drag will still be some fraction of the value found using eq. (14), although a more refined calculation is needed to predict the fraction quantitatively.

If the DF drag becomes inefficient when the orbit reaches the protogalaxy core and becomes subsonic, then these massive black holes may have more time to grow by accretion before they finally sink to the centers of their host galaxies.

Finally, we comment on the applicability of our results to the interaction of protoplanets with a gaseous circumstellar nebula in which they may grow. Protoplanets orbit faster than the surrounding gaseous nebula, with the Mach number of the drift speed  $\mathcal{M} \equiv v_{\text{rel}}/c_s \approx c_s/(\Omega_K r) \ll 1$  (where  $\Omega_K$  is the local Kepler angular rotation frequency and  $r$  is the protoplanet's semimajor axis). Drag forces occur as a result of this relative motion, which leads to inward radial migration of protoplanets as they lose angular momentum to the surrounding nebula (see, e.g., Ward 1997 and references therein). Using parameters based on solid bodies in the protosolar nebula, it can be shown that the nominal DF drag from equations (12) and (14),  $F_{\text{DF}} \approx (4\pi/3)(GM_p)^2 \rho_0 / (c_s \Omega_K r) \approx (2\pi/3)(GM_p)^2 \Sigma / (c_s^2 r)$ , exceeds the large Reynolds number aerodynamic drag  $F_{\text{aer}} \approx (1/4)v_{\text{rel}}^2 \pi R_p^2 \rho_0$  (§ 45 of Landau & Lifshitz 1987) for protoplanets of radius  $R_p$  greater than a few hundred km.

It is sometimes argued that gravitationally enhanced drag on protoplanets (see, e.g., Takeda et al. 1985; Ohtsuki, Nakagawa, & Nakazawa 1988, but note the different

scaling from our results) may enhance migration rates over those predicted to arise from differential resonant torques (Goldreich & Tremaine 1980) between the protoplanet and the surrounding nebula. In fact, provided that the difference of gas orbits from Kepler orbits is included so that the perturber does not corotate with the nebular gas at the same radial distance, then the DF drag is automatically incorporated in the net resonant torque. Indeed, calculations show that the net resonant torque from a thin disk (see, e.g., Korycansky & Pollack 1993; Ward 1997), taking this velocity difference into account, is of the same magnitude (and scaling) as the DF drag estimated above. Thus, while the gaseous DF drag may have implications for the late stages of planet formation, its effects are naturally incorporated within a full resonant formalism. Although such a calculation has not yet been performed in three dimensions, it is reassuring that our simple estimate of the drag—which neglects gradients of velocity, density, and temperature in the disk—and the estimates from two-dimensional resonant torque differences—which neglect the disk thickness—nevertheless yield comparable answers.

The author is grateful to the referee, Scott Tremaine, for helpful comments on the manuscript.

#### REFERENCES

- Binney, J., & Tremaine, S. 1987, *Galactic Dynamics* (Princeton: Princeton Univ. Press)
- Bondi, H., & Hoyle, F. 1944, *MNRAS*, 104, 273
- Chandrasekhar, S. 1943, *ApJ*, 97, 255
- Dokuchaev, V. P. 1964, *Soviet Astron.*, 8, 23
- Goldreich, P., & Tremaine, S. 1980, *ApJ*, 241, 425
- Hillenbrand, L. A. 1997, *AJ*, 113, 1733
- Hillenbrand, L. A., & Hartmann, L. W. 1998, *ApJ*, 492, 540
- Hoyle, F., & Lyttleton, R. A. 1939, *Proc. Cambridge Philos. Soc.*, 35, 405
- Hunt, R. 1971, *MNRAS*, 154, 141
- Jackson, J. D. 1975, *Classical Electrodynamics* (New York: Wiley)
- Just, A., & Kegel, W. H. 1990, *A&A*, 232, 447
- Korycansky, D. G., & Pollack, J. B. 1993, *Icarus*, 102, 150
- Landau, L. D., & Lifshitz, E. M. 1987, *Fluid Mechanics* (Oxford: Pergamon)
- Marshall, J., Ostriker, E., & Teuben, P. 1999, in preparation
- Ohtsuki, K., Nakagawa, Y., & Nakazawa, K. 1988, *Icarus*, 75, 552
- Ostriker, J. P., & Davidsen, A. F. 1968, *ApJ*, 151, 679
- Rephaeli, Y., & Salpeter, E. E. 1980, *ApJ*, 240, 20
- Ruderman, M. A., & Spiegel, E. A. 1971, *ApJ*, 165, 1
- Ruffert, M. 1996, *A&A*, 311, 817
- Saiyadpour, A., Deiss, B. M., & Kegel, W. H. 1997, *A&A*, 322, 756
- Shankar, A., Kley, W., & Burkert, A. 1993, *A&A*, 274, 955
- Shima, E., Matsuda, T., Hidenori, T., & Sawada, K. 1985, *MNRAS*, 217, 367
- Silk, J., & Rees, M. J. 1998, *A&A*, 331, L1
- Takeda, H., Matsuda, T., Sawada, K., & Hayashi, C. 1985, *Prog. Theor. Phys.*, 74, 272
- Tremaine, S., Ostriker, J. P., & Spitzer, L. 1975, *ApJ*, 196, 407
- Ward, W. R. 1997, *Icarus*, 126, 261